Comparison of molecular models of carbon monoxide for calculation of vapor-liquid equilibrium

Comparación de modelos moleculares del monóxido de carbono para el cálculo del equilibrio líquido-vapor

Bibian Alonso Hoyos-Madrigal[*]*, Farid Chejne-Janna*

Departamento de Procesos y Energía, Facultad de Minas, Universidad Nacional de Colombia (Sede Medellín). Carrera 80 N.º 65-223. A.A. 1027. Medellín, Colombia.

(Received April 02, 2014; accepted March 02, 2015)

Abstract

There are a number of molecular models for carbon monoxide developed from different experimental measurements. This paper aims to compare the results that several of these models produced in the calculation of vapor-liquid equilibrium, in order to recommend which model should be used according to the property and phase to be calculated. The selected models included four non-polar models, with one or two Lennard-Jones sites, and four polar models with dipoles or partial charges to represent the polarity of carbon monoxide. Gibbs-ensemble Monte Carlo simulations in the canonical version (NVT-GEMC) were used to determine the densities of the phases in equilibrium, the vapor pressure and vaporization enthalpy between 80 and 130 K with each of the selected models. It was found that the more complex molecular models, SVH, ANC and PGB, better described the density of the saturated liquid (about 7% average deviation), but these models generated deviations higher than 40% for vapor properties and 20% for vaporization enthalpy. On the other hand, the non-polar BLF model generated the lowest deviations for saturation pressure and vapor density (6.8 and 21.5%, respectively). This model, as the model HCB, produces acceptable deviations for liquid density and vaporization enthalpy (between 10 and 12%). The BLF and HCB models, being non-polar and not requiring the calculation of long-range interactions, can be considered as the molecular models presenting the most satisfactory balance between deviations of the results and calculation complexity.

----------*Keywords:* molecular models, thermodynamic properties, vapor-liquid equilibrium, carbon monoxide

* Corresponding author: Bibian Alonso Hoyos Madrigal, e-mail: bahoyos@unal.edu.co
DOI: 10.17533/udea.redin.n75a14

Resumen

Existen varios modelos moleculares para el monóxido de carbono desarrollados a partir de diferentes mediciones experimentales. El objetivo de este trabajo es comparar los resultados que varios de estos modelos producen en el cálculo del equilibrio líquido-vapor en busca de recomendar qué modelo debe ser usado de acuerdo la propiedad y la fase que se desea calcular. Los modelos seleccionados corresponden a cuatro modelos no polares, con uno o dos sitios Lennard-Jones, y cuatro modelos polares, con dipolos o cargas parciales para representar la polaridad del monóxido de carbono. Simulaciones Monte Carlo en la versión Gibbs canónica (NVT-GEMC) se emplearon para determinar las densidades de las fases en equilibrio, la presión de vapor y la entalpia de vaporización entre 80 y 130 K con cada uno de los modelos seleccionados. Se encontró que los modelos más complejos SVH, ANC y PGB, son los que mejor describen la densidad del líquido saturado (alrededor de 7% de desviación promedio), pero estos modelos generan desviaciones mayores al 40% para las propiedades del vapor y al 20% para la entalpia de vaporización. Por otro lado, el modelo no-polar BLF generó las menores desviaciones para la presión de saturación y la densidad del vapor (6.8 y 21.5%, respectivamente). Este modelo, al igual que el modelo HCB, produce desviaciones aceptables para la densidad del líquido y la entalpia de vaporización (entre 10 y 12%). Los modelos no polares BLF y HCB, que no requieren el cálculo de las interacciones de largo alcance, se pueden considerar como los modelos moleculares que presentan un balance satisfactorio entre desviaciones en los resultados y complejidad de cálculo.

----------*Palabras clave:* modelos moleculares, propiedades termodinámicas, equilibrio L-V, monóxido de carbono

Introduction

In recent years, the availability of more powerful systems of calculation has opened the possibility of calculating data for thermodynamic and transport properties from simulations with molecular models. These molecular simulations allow the extraction of structural, thermodynamic and dynamic information on macroscopic phenomena from the description of microscopic molecular interactions. The correct description of these molecular interactions leads to a better understanding and interpretation of experimental results and allows to interpolate or extrapolate the results to conditions that may be inaccessible in the laboratory, which confers to these models a greater physical meaning and an excellent predictive power [1-2].

A correct description of the molecular structure and the study of the thermodynamic properties of carbon monoxide are of great importance due to the role of this substance in many industrial processes, and because it is an important byproduct in the production of formic acid, polyurethane, polycarbonates and methylacrylates; it is also present in the combustion gases of internal combustion engines and in fuel cells fed with products of reformed hydrocarbons and alcohols (applications for which require the study of the adsorption of CO in catalysts) and in its application as an additive for the storage of meat products.

Although carbon monoxide initially appears to be an easy-to–model molecule, the construction of a molecular model suitable for describing its

behavior over a wide range of conditions has not been fully achieved because this molecule has a polarity (C^-O^+) [3, 4] opposite of the more intuitive configuration (C^+O^-). Additionally, the fact that it possesses a small dipole moment (0.112 D), a moderate internal polarization (3.5 D Å^2) and a large quadrupole moment (- 2.45 D Å) confers characteristics that are difficult to model, especially for the correct description of the solid state and for adsorption at low temperatures [5].

There are a large number of molecular models used to represent the CO molecule. Within the simpler non-polar models are those that represent the CO molecule as a spherical Lennard–Jones site without charges (1CLJ), developed mainly from viscosity data [6-8] or the second virial coefficient [9-11], although in recent years, these models have also been used to study the separation of CO and H_2 on carbon nanotubes [12]. Another model proposes a rigid molecule composed of two equal L-J centers (2CLJ) located at each atom [13], which has been used to study the thermal conductivity of liquid CO [14] and its solubility in ionic liquids [15].

Polar models present a broader spectrum; first, there are the Stockmayer models (L-J spheres with a dipole or a quadrupole embedded in their centers) [16, 17]. Extensions of this model consist of 2CLJ models with symmetrical centers and a dipole or a quadrupole located at the center of the molecule [18], and there are even 2CLJ models with asymmetric centers containing both a dipole and a quadruple that had been used to study the composition of planetary atmospheres [19].

In another group of polar models, partial charges are used instead of dipoles or quadrupoles. Among these models are those that approximate the experimental dipole moment but do not consider the quadrupole moment; these models are composed of 2CLJ with two charges of equal magnitude and opposite sign located at each site (2CLJ2q), and they have been mainly used for CO adsorption studies on coal structures such as graphite and fullerenes [20-23]. Continuing in complexity, there are models that represent the quadrupole moment with three charges in the molecule (2CLJ3q), one at each end and one in the center of the molecule, of opposite sign and equal to the sum of the other two. 2CLJ3q models have been mainly used in studies of the dynamics of the photo-dissociation of CO from myoglobin protein [24-27]; also, more complex models of five sites, used for simulations of the structure of solid CO, have been proposed [28, 29].

Many of the abovementioned models may not be appropriate for calculating the vapor-liquid equilibrium (VLE) because they were designed for other applications, such as investigations of the structure in the liquid phase, adsorption studies at low temperatures or the description of the second virial coefficient, and they may produce poor results when applied in equilibrium calculations.

The objective of this work was to evaluate the results generated by several of these molecular models when used for the calculation of VLE thermodynamic properties of carbon monoxide using Monte Carlo simulations. The evaluation of the models was not exhaustive in terms of the number of models (which would require an enormous computational effort to undertake); rather, the scope herein is restricted to models representing each of the families described above. The evaluation of these models in calculating the VLE was not intended to absolutely validate or invalidate the models, as they were evaluated with a calculation for which. in general, they were not designed; we intended merely to verify the robustness of the models for different types of calculations.

Simulation details

Molecular models

For this evaluation, four non-polar and four polar models were selected. Two of the non-polar models (here designated HCB [6] and RPP [8], respectively) consist of spherical centers in which the interactions between particles are calculated by the Lennard-Jones potential (Eq. 1):

$$\psi_{LJ}(r_{ij}) = 4\varepsilon\left\{\left(\frac{\sigma}{r_{ij}}\right)^{12} - \left(\frac{\sigma}{r_{ij}}\right)^{6}\right\} \quad (1)$$

where ε and σ represent the depth and the position of the potential well, respectively, and r_{ij} is the distance between the centers of the molecules.

The third model corresponds to the 2CLJ potential of Bohn [13] (commonly known as the BLF model), which describes the carbon monoxide molecule as a combination of two equal Lennard-Jones sites (located on the oxygen and carbon atoms), separated by a bond distance *d,* (Eq. 2):

$$\psi_{2CLJ} = \sum_{a=1}^{2}\sum_{b=1}^{2}\psi_{LJ}(r_{ia,jb}) \quad (2)$$

where *a* and *b* denote sites belonging to molecule *i* or *j*, respectively, and $r_{ia,\,jb}$ denotes the distance between site *a* of molecule *i* and site *b* of molecule *j*.

The other non-polar model (ANC) was developed from an approximated non-conformal theory [11] and has a functional form that corresponds to a modified Kihara potential (Eq. 3):

$$\psi_{ANC} = \varepsilon\left[\left(\frac{1-a_0}{\xi_{ij}-a_0}\right)^{12} - 2\left(\frac{1-a_0}{\xi_{ij}-a_0}\right)^{6}\right] \quad (3)$$

With (Eq. 4)

$$\xi_{ij} = \sqrt[3]{1 + \frac{\left(r_{ij}/\sigma\right)^{3} - 1}{s}} \quad (4)$$

and the constant $a_0 = 0.095739$.

This model, in addition to the parameters *ε* and σ, uses a third parameter (*s*) called the effective softness of the molecule.

The parameter a_0 is determined in such a way that Eq. (3) reproduces the pair potential of argon (to which the value *s*=1 was assigned). The increase in the value of *s* in Eq. (3) produces potentials that are less steep (i.e., softer) than the potential of the reference atom (argon).

It should be noted that the HCB and RPP models require only two parameters (ε and σ) and the ANC and BLF models require an additional parameter (*s* and *d*, respectively). The values of the parameters for each of these potential models are shown in Table 1.

Table 1 Parameters for the potential models. ε/k_B (K), σ (Å), *d* (Å), *μ* (D) and *q* (e)

Model	*Parameters*	*Reference*
HCB	ε/k_B = 110 σ = 3.59	[6]
RPP	ε/k_B = 91.7 σ = 3.69	[8]
BLF	ε/k_B = 42.282 σ = 3.2717 d = 1.276	[13]
ANC	ε/k_B = 145.246 σ = 3.95952 s = 0.8876	[11]
Stockmayer	ε/k_B = 101.2 σ = 3.623 μ = 0.11167	[17]
SVH	ε/k_B = 36.897 σ = 3.3009 d = 1.1405 μ = 0.7378	[18]
PGB	ε_{CC}/k_B = 37.15 σ_{CC} = 3.55 ε_{OO}/k_B = 61.57 σ_{OO} = 2.95 d = 1.128 q = 0.0223	[23]
SK	ε_{CC}/k_B = 13.19 σ_{CC} = 3.83 q_C = -0.75 ε_{OO}/k_B = 80.09 σ_{OO} = 3.12 q_O = -0.85 d = 1.128 q_{cm} = 1.6	[26]

Of the four selected polar models, two use dipoles at their centers, and the other two make use of partial charges located on the atoms.

The models that use dipoles correspond to the Stockmayer model, composed of 1CLJ with a dipole (μ) in the center [17] and an extension of that presented by Stoll [18] (model SVH) that consists of an identical 2CLJ with a dipole at the geometric center of the molecule.

For these models, the potential is (Eq. 5):

$$\psi = \psi_{LJ} + \psi_D \quad (5)$$

in which is the L-J potential for one or two sites, according to the respective cases, and is the dipole contribution given by (Eq. 6):

$$\psi_D = \frac{1}{4\pi\epsilon_0}\frac{\mu^2}{\left|\boldsymbol{r}_{ij}\right|^3}(\cos\gamma_{ij} - 3\cos\theta_i\cos\theta_j) \quad (6)$$

where is the vacuum permittivity, θ_i and θ_j are the angles formed between the dipole vectors $\boldsymbol{\mu}_i$ and $\boldsymbol{\mu}_j$ of molecules *i* and *j*, respectively, with the vector $\boldsymbol{r}_{ij}$ between the centers of the molecules and γ_{ij} is the angle between the dipole vectors $\boldsymbol{\mu}_i$ and $\boldsymbol{\mu}_j$. In developing the SVH model, the magnitude of the dipole was considered an adjustable parameter, yielding a value μ= 0.7378 D, which is significantly higher than the experimental value.

The third polar model (PGB model [23]) consists of two different L-J centers and two partial charges, each with a value of 0.0223 *e*, negative at the oxygen atom and positive at the carbon. These charge values produce a dipole of 0.12 D, which is very close to the experimental value.

Finally, the fourth polar model is the 2CLJ3q model developed by Straub and Karplus (commonly called the SK model) [26], which consists of asymmetric charges and L-J interaction sites located on the oxygen and carbon atoms (separated by a distance *d*) and an additional charge placed at the center of mass of the molecule. This model allows differentiating the carbon and oxygen atoms, which is an advantage in structural studies of CO adsorption on surfaces. Additionally, the SK model reproduces ab initio (Hartree-Fock) interaction energies of CO with water, methanol, imidazole and formamide, gives an excellent lattice constant and sublimation enthalpy for solid CO, yields the hydration free energy of CO and quantitatively reproduces the vibrational frequencies of CO with an RRKR potential.

For the PGB and SK models, the potential is (Eq. 7):

$$\psi = \psi_{2CLJ} + \psi_q \quad (7)$$

in which is the long-range contribution due to the presence of the charges, given by (Eq. 8):

$$\psi_q = \frac{1}{4\pi\epsilon_0}\sum_{a=1}^{N_q}\sum_{b=1}^{N_q}\frac{q_i^a q_j^b}{r_{ia,jb}} \quad (8)$$

Here, N_q is the number of charges in the molecule, and is the charge on site *a* of molecule *i*.

As can be observed, the SK model has eight parameters, the PGB model has six (ε_{CC}, ε_{OO}, σ_{CC}, σ_{OO}, *d* and *q*), the SVH model has four parameters (ε, σ, *d* and μ) and the Stockmayer model has only three (ε, σ and μ). The parameters of the polar potential models are also shown in Table 1.

For the PBG and SK models, the cross interactions between different sites of the carbon monoxide molecule were calculated using the Lorentz-Berthelot mixing rules [30], (Eqs. 9 and 10).

$$\sigma_{CO} = \frac{1}{2}(\sigma_{CC} + \sigma_{OO}) \quad (9)$$

$$\varepsilon_{co} = (\varepsilon_{cc}\varepsilon_{oo})^{\frac{1}{2}} \quad (10)$$

Technical details

The Gibbs-ensemble Monte Carlo (GEMC) method is particularly suitable for direct simulations of phase equilibrium [31]. Therefore, the canonical version (NVT-GEMC) was used to determine the properties at equilibrium.

In the Gibbs ensemble, two phases in equilibrium are simulated at a given temperature and with a

constant total number of molecules. Procedurally, the simulation starts in an unstable or meta-stable region that is subsequently divided into two subsystems. In the course of the simulation, the system forms two homogenous phases from the separated subsystems. The phase separation is carried out by three types of movements, which include changes in the position and orientation of molecules randomly chosen in each phase (to assure the equilibrium within each region), particle exchange between the coexisting phases (to equilibrate the chemical potentials of the components in each phase) and changes in the volume of each phase (to equilibrate the pressures).

For this work, six points of the VLE with each of the selected models were calculated. The temperature was varied between 80 and 130 K at intervals of 10 K. In all the simulations, 512 molecules of CO were used (which involves 1,024 sites for the 2CLJ models), with periodic boundary conditions in three dimensions, with a cutoff radius of 2.5σ and long-range (tail) corrections for the L-J potential beyond the spherical cutoff. In all, 2×10^6 equilibration cycles and other 2×10^6 production cycles were used. Each Monte Carlo cycle is defined here as N attempts to move a molecule, N attempts to exchange particles between the phases and an attempt to change the volume (for the 2CLJ or dipole models, *2/3N* attempts of rotation of the molecule or the dipole were added). The order in which the attempts were conducted was selected at random.

The generation of a new configuration at the volume-change stage was performed using a random path in $ln(V_1/V_2)$ [31], the change in the orientation of the molecules was made using the Jansoone method [30], and the magnitude of this change and the magnitude of change in the displacement were adjusted to produce an acceptance of approximately 50% of the attempts. In the simulations with the polar models, Ewald sums were used to calculate long-range interactions.

Near the critical point (130 K), the simulations are quite unstable and all models required at least 5×10^5 cycles to achieve equilibrium; for lower temperatures, the simulations are more stable and less than 1×10^5 cycles were required.

The residual energy (Eq. 11), and density (Eq.12) of each phase were obtained as ensemble averages over the production period:

$$U_R^{\alpha} = \langle \sum_{i<j} \psi^{\alpha} \rangle \tag{11}$$

$$\rho^{\alpha} = \langle \frac{N^{\alpha}}{V^{\alpha}} \rangle \frac{1}{N_A} \tag{12}$$

In these equations, the brackets denote the ensemble average and U_R^{α}, ρ^{α} and V^{α} are the residual energy, density and volume of phase α, respectively, and N_A is Avogadro's number.

The pressure was determined by calculating the internal virial (Eq. 13):

$$P^{\alpha} = k_B T \rho^{\alpha} + \langle \frac{\mathcal{W}^{\alpha}}{V^{\alpha}} \rangle \tag{13}$$

where k_B is the Boltzmann constant, T is the temperature and (Eq.14), is the intermolecular virial function of the phase α, defined as :

$$\mathcal{W} = -\frac{1}{3} \sum_i \sum_{j>i} \boldsymbol{r}_{ij} \cdot \nabla\psi = \frac{1}{3} \sum_i \sum_j \mathcal{w}_{ij} \tag{14}$$

The expressions for the pair-intermolecular virial functions ($\mathcal{w}_{ij}$) for each type of potential are shown in the Appendix.

Because the results calculated for the pressure of the liquid phase usually show large fluctuations, the reported pressure values are those of the vapor phase.

As the degrees of freedom by rotation, translation and vibration of molecules in each phase are equal, the vaporization enthalpy (Eq. 15), can be calculated as the difference between the residual enthalpy of the liquid and vapor phases:

$$\Delta h^v = U_R^v - U_R^l + P^v\left(\frac{1}{\rho^v} - \frac{1}{\rho^l}\right) \qquad (15)$$

The results of the calculation of the properties produced by the simulations were compared with data reported in the REFPROP database [32], and the average relative deviations (δ_{rel}) were calculated by (Eq. 16):

$$\delta_{rel}^2 = \frac{1}{N_D}\sum_{i=1}^{N_D}\left[\left(1 - \frac{\langle A\rangle}{A_{Exp}}\right) * 100\right]^2 \qquad (16)$$

where N_D = 6 is the number of VLE points calculated and A represents the properties density, pressure and enthalpy.

Results and discussion

The comparison between simulation results and experimental data for the VLE of carbon monoxide is shown in Figures 1 to 5. Table 2 lists the results of the relative average deviations of each model in the calculation of the densities of the phases, the vapor pressure and the vaporization enthalpy.

The results of the VLE predictions of the non-polar models (Figure 1 and Table 2) show that, in the liquid phase, the ANC model presented the lowest average deviation (7.1%) followed by the HCB and BLF models (10.1 and 11.6%, respectively). It can also be observed that the RPP model produced the smallest equilibrium curve of all the models (i.e., it significantly underestimates the liquid density and overestimates the vapor density) and tended to produce a constant density of the liquid for temperatures above 100 K. The statistical uncertainties of these models for the values of liquid density were between 0.2 and 4%, and the deviations from the experimental data fell outside this range of uncertainty.

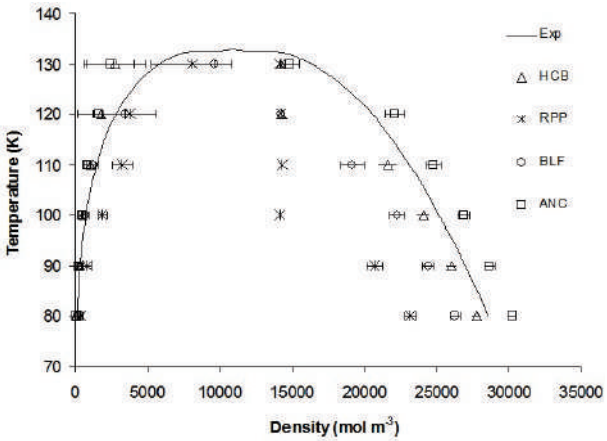

Figure 1 Results for VLE of carbon monoxide with non-polar models. Error bars not shown are smaller than the symbol size

Table 2 Relative average deviations of thermodynamic properties of VLE obtained with the molecular models of carbon monoxide

	Relative average deviations (%)			
Model	***ρl***	***ρv***	***Pv***	***Δh v***
HCB	10.1	30.9	41.2	9.7
RPP	28.0	114.1	289.2	35.1
BLF	11.6	21.5	6.8	11.8
ANC	7.1	47.9	38.7	23.3
Stockmayer	18.3	34.7	104.6	29.3
SVH	6.6	145.2	67.2	21.5
PGB	6.9	66.4	59.8	27.1
SK	14.7	39.8	48.3	23.6

In the vapor phase, the average deviations were much higher than in the liquid phase; here, the BLF model produced the best estimation, with deviations between 6 and 20% for temperatures between 80 and 120 K, but with a much larger deviation around the critical point (64.1% at 130 K). However, the BLF model presented the lowest average deviation over the whole range of temperatures studied (21.5%). The statistical uncertainties for this phase were also higher than in the liquid phase (between 30 and 80%), especially at low temperatures due to the small values of the density at these points.

Figure 2 shows the densities of the phases in equilibrium produced by the polar models. For the liquid phase, the statistical uncertainties obtained from these models were very similar to those generated with the non-polar models (between 0.5% and 4%), although the SVH and SK models presented uncertainties of about 15% for temperatures above 120 K. The average deviations between the values generated by these models and the experimental data for the liquid phase were slightly lower than 7% for the SVH and PGB models and between 15 and 18% for the SK and Stockmayer models. As with the non-polar models, in most cases these differences were outside of the range of statistical uncertainties.

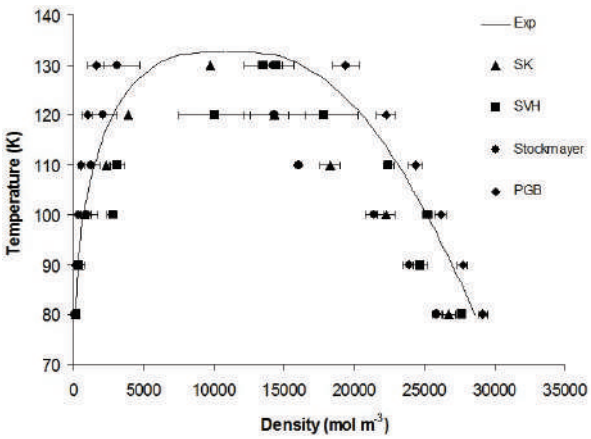

Figure 2 Results for VLE of carbon monoxide with polar models. Error bars not shown are smaller than the symbol size

In the vapor phase, the Stockmayer model produced the lowest average deviation of the polar models (34.7%), and, as with the non-polar models, the statistical uncertainties for this phase were higher than in the liquid phase (between 30 and 80%).

In general, the SVH and SK models exhibited the opposite behavior; the SVH model better reproduced the liquid density, while the SK model was better for the vapor. This difference in behavior can be attributed to, in addition to the differences in the parameters of the models, the calculation of the Ewald sums, which is less stable when using dipoles instead of point charges. This effect can also be observed in the high statistical uncertainties of the Stockmayer model.

Figures 1 and 2 show that, while the ANC and PGB models produced liquid-density values higher than the experimental data, the other models produced lower liquid densities. In general, the SVH, PGB and ANC models better reproduced the liquid density (with average deviations of around 7%, as shown in Table 2), but the ANC and PGB models significantly underestimated the vapor density over the whole range of temperatures analyzed, while the SVH model overestimated the vapor-density values, showing large deviations in the region near the critical point. The Stockmayer model overestimated the vapor density for temperatures lower than 100 K and tended to underestimate it at higher temperatures.

Although HCB was not the model that best reproduced the density values of each phase in equilibrium, it is the model that best estimated the change in density of vaporization (ρ^l - ρ^v), as shown in Figure 3. This figure also shows the large deviations in the SVH model near the critical point and those of the RPP model over virtually the entire range of temperatures. For the ANC and PGB models, the deviations were mainly generated by the low vapor-density values.

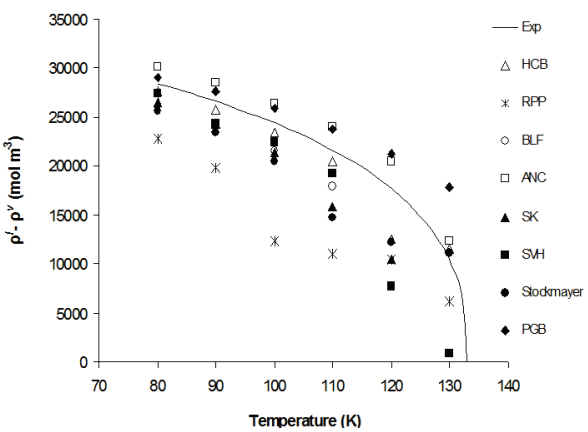

Figure 3 Comparison of results of vaporization density change for carbon monoxide (ρ^l - ρ^v). Error bars have been omitted for clarity

Figure 4 shows a comparison between the results for saturation pressure generated by each model and the experimental data. The BLF model produced an excellent adjustment over the entire temperature range, with deviations between 5.5 and 9.1% (average deviation of 6.8%). All other models produced values of vapor pressure with deviations exceeding 35%; the RPP and Stockmayer models even produced deviations around 100 and 300%, respectively. Except for the RPP model, all other non-polar models produced deviations lower than the polar models in calculating the vapor pressure.

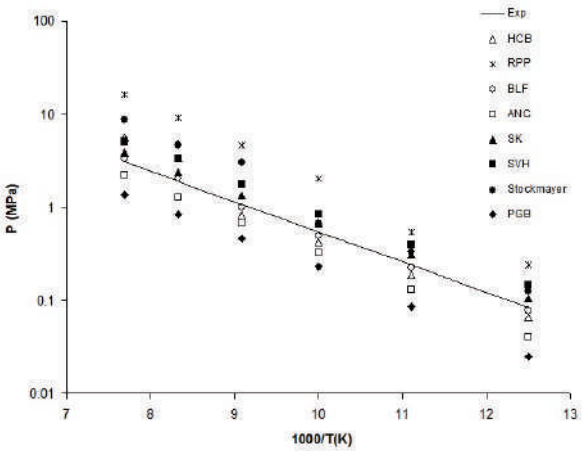

Figure 4 Comparison of results of vapor pressure for carbon monoxide. Error bars have been omitted for clarity

The enthalpy of vaporization calculated with each model is shown in Figure 5. It can be seen that the non-polar models HCB and BLF, with average deviations of 9.7% and 11.7%, respectively, better reproduced the vaporization enthalpy. For all other models, the deviations were higher than 20%. These larger deviations can be attributed not only to deviations arising from vapor pressure deviations but also to large deviations in vapor density and residual energy. This is evident in models such as the ANC, which, although it underestimated the vapor pressure, overestimated the vaporization enthalpy over the entire range of temperatures, due to its low values for vapor density. The PGB model, which also underestimated the saturation pressure and the vapor density, showed a small variation in the residual energies of the phases, leading to this model to produce lower values of vaporization enthalpy for temperatures between 80 and 100 K and higher vaporization enthalpies at higher temperatures. For the RPP model, the large underestimation in vaporization enthalpy can be attributed mainly to the large deviations in the densities of the two phases in equilibrium.

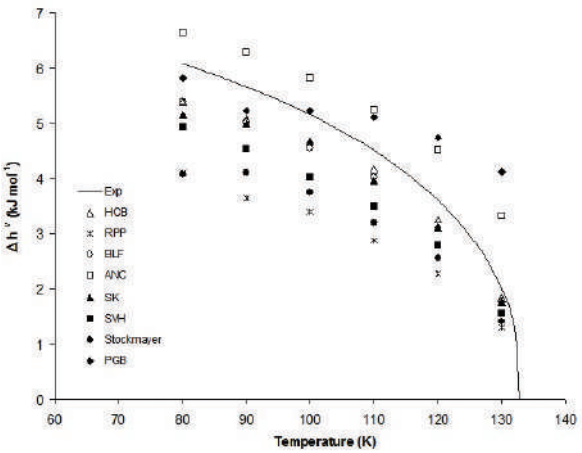

Figure 5 Comparison of results of vaporization enthalpy for carbon monoxide. Error bars have been omitted for clarity

The analysis of results can be finalized by saying that the liquid phase is best described by SVH and PGB models because these models take into account explicitly the interactions that happen to be more relevant in the condensed phase. That is, when considering the electrostatic interactions with farther molecules. Furthermore, the SK model with three charges, considers a greater electrostatic interaction, which in turn generates a larger deviation in liquid density calculations. In the non-polar ANC model, interactions in the liquid phase are supplemented from the effective softness parameter that allows considering the effects of proximity of neighboring molecules.

Although the magnitude of the electrostatic interactions contained in the SVH and PGB models allow a better description of the liquid

phase, unfortunately this also generates a not appropriate description of vapor phase. In general these models, as well as the SK model, should not be used to calculate the vapor phase.

The non-polar RPP model has a relatively low energy parameter for a single-site model, which generates large deviations in the results and therefore, should not be used for calculation of vapor-liquid equilibrium.

It is important to note here that the HCB and BLF models, besides better describing the vapor density, saturation pressure and vaporization enthalpy, have the advantage that the simulations are carried out relatively rapidly, as they do not require the calculation of long-range interactions. The HCB model has the additional advantage of requiring only two parameters for describing the carbon monoxide molecule.

Conclusions

The results of the calculation of thermodynamic properties of the VLE of carbon monoxide with four polar and four non-polar molecular models were compared.

The BLF and HCB models, while producing slightly higher deviations than the ANC, PGB and SVH models in the calculation of saturated liquid density, still better predicted the pressure and density of the equilibrium vapor phase and the vaporization enthalpy. The BLF and HCB models, being non-polar models and not requiring the calculation of long-range interactions, can be considered as the molecular models presenting the most satisfactory balance between small deviations of the results and reduced calculational complexity.

Among the models studied, the ANC, PGB and SVH models best predicted the saturated liquid density of carbon monoxide, but these models showed large deviations in the saturation pressure, vapor density and vaporization enthalpy. The RPP model produced the largest deviations in the calculation of equilibrium properties.

Acknowledgments

The authors wish to thank the Unidad de Cálculo Numérico avanzado de la Universidad Nacional de Colombia-Medellín (Advanced Numeric Calculation Unit at the National University of Colombia-Medellín) for the time given for completion of the simulations.

Appendix

The intermolecular-pair virial function is defined here as (Eq. 17):

$$w = -r\frac{d\psi}{dr} \tag{17}$$

For the ANC model, it is (Eq. 18):

$$w_{ij}^{ANC} = \frac{12\varepsilon r_{ij}^3}{s\xi_{ij}^2(\xi - a_0)}\left[\left(\frac{1-a_0}{\xi - a_0}\right)^{12} - \left(\frac{1-a_0}{\xi - a_0}\right)^{6}\right] \tag{18}$$

For models that use only L-J interactions (models HCB, RPP and BLF), it is (Eq. 19):

$$w_{ij}^{LJ} = 48\varepsilon\left[\left(\frac{\sigma}{r_{ij}}\right)^{12} - \frac{1}{2}\left(\frac{\sigma}{r_{ij}}\right)^{6}\right] \tag{19}$$

For the models containing dipoles (Stockmayer and SVH), it is (Eq. 20):

$$w_{ij} = w_{ij}^{LJ} + \frac{w_{ij}^{D}}{4\pi\epsilon_0} \tag{20}$$

with (Eq. 21)

$$w_{ij}^{D} = \left(\boldsymbol{\mu}_i \cdot \boldsymbol{\mu}_j\right) D_{ij} - \left(\boldsymbol{\mu}_i \cdot \boldsymbol{r}_{ij}\right)\left(\boldsymbol{\mu}_j \cdot \boldsymbol{r}_{ij}\right) E_{ij} +$$

$$\frac{4\pi}{V}\sum_{\mathbf{k}\neq 0}\left[\left(\boldsymbol{\mu}_i \cdot \mathbf{k}\right)\left(\boldsymbol{\mu}_j \cdot \mathbf{k}\right)\frac{exp\left(-\frac{\mathrm{k}^2}{4\beta^2}\right)}{\mathrm{k}^2}\left(\mathbf{k} \cdot \boldsymbol{r}_{ij}\right)\sin\left(\mathbf{k} \cdot \boldsymbol{r}_{ij}\right)\right] \tag{21}$$

where β is the parameter of the width of the charge distribution and $\boldsymbol{k}$ are the vectors of the reciprocal space used in the Ewald sums, and D_{ij} and E_{ij} are given by Eqs. 22 and 23, respectively.

$$D_{ij} = \frac{3\ erfc(\beta r_{ij})}{r_{ij}^3} + \frac{2\beta exp\left(-(\beta r_{ij})^2\right)}{\pi^{1/2}}\left(2\beta^2 + \frac{3}{r_{ij}^2}\right) \quad (22)$$

$$E_{ij} = \frac{15\ erfc(\beta r_{ij})}{r_{ij}^5} + \frac{2\beta exp\left(-(\beta r_{ij})^2\right)}{\pi^{1/2}} \left[\frac{15}{r_{ij}^4} + \frac{4\beta^2}{r_{ij}^2} + 2\beta^2\left(2\beta^2 + \frac{3}{r_{ij}^2}\right)\right] \quad (23)$$

For models with partial charges (Eq. 24):

$$w_{ij} = w_{ij}^{LJ} + \frac{w_{ij}^q}{4\pi\epsilon_0} \quad (24)$$

with w_{ij}^q given by (Eq. 25)

$$w_{ij}^q = q_i q_j \left(\left[\frac{2\beta exp\left(-(\beta r_{ij})^2\right)}{\pi^{1/2}} + \frac{erfc(\beta r_{ij})}{r_{ij}}\right] + \sum_{\mathbf{k}\neq 0}\left[\frac{exp\left(-\frac{\mathrm{k}^2}{4\beta^2}\right)}{\mathrm{k}^2}\left(\mathbf{k}\cdot\boldsymbol{r}_{ij}\right)\sin\left(\mathbf{k}\cdot\boldsymbol{r}_{ij}\right)\right]\right) \quad (25)$$

References

1. J. Pablo, F. Escobedo. "Molecular simulations in chemical engineering: Present and future". *AIChE J*. Vol. 48. 2002. pp. 2716-2721.
2. W. Gunsteren, H. Berendsen. "Computer Simulation of Molecular Dynamics: Methodology, Applications, and Perspectives in Chemistry". *Angew. Chem. Int. Ed. Engl*. Vol. 29. 1990. pp. 992-1023.
3. W. Meerts, F. Leeuwm, A. Dymanus. "Electric and magnetic properties of carbon monoxide by molecular-beam electric-resonance spectroscopy". *Chem. Phys*. Vol. 22. 1977. pp. 319-324.
4. J. Muenter. "Electric dipole moment of carbon monoxide". *J. Mol. Spectrosc*. Vol. 55. 1975. pp. 490-491.
5. W. Steele. "Monolayers of linear molecules adsorbed on the graphite basal plane: structures and intermolecular interactions". *Langmuir*. Vol. 12. 1996. pp. 145-153.
6. J. Hirschfelder, C. Curtiss, R. Bird. *Molecular theory of gases and liquids*. 1st ed. Ed. Wiley. New York, USA. 1964. pp. 1112-1116.
7. R. Bird, W. Stewart, E. Lighfoot. *Transport Phenomena*. 2nd ed. Ed. Wiley. New York, USA. 2002. pp. 863-866.
8. R. Reid, J. Prausnitz, B. Poling. *The properties of gases and liquids*. 4th ed. Ed. McGraw-Hill. Singapore, Singapore. 1988. pp. 733-734.
9. J. Ramos, F. Río, I. McLure. "Nonconformal potentials and second virial coefficients in molecular fluids. II. Applications to nonspherical molecules". *J. Phys. Chem. B*. Vol. 102. 1998. pp. 10576-10585.
10. F. Río, J. Ramos, I. McLure. "Nonconformal potentials and second virial coefficients in molecular fluids. I. Theory". *J. Phys. Chem. B*. Vol. 102. 1998. pp. 10568-10575.
11. J. Ramos, F. Río. I. McLure. "Accurate effective potentials and virial coefficients in real fluids - Part IV. Heterodiatomic and polyatomic substances with permanent multipoles and their mixtures with noble gases". *Phys. Chem. Chem. Phys*. Vol. 3. 2001. pp. 2634-2643.
12. C. Gu, G. Gao, Y. Yu, T. Nitta. "Simulation for separation of hydrogen and carbon monoxide by adsorption on single-walled carbon nanotubes". *Fluid Phase Equilibria*. Vol. 194-197. 2002. pp. 297-307.
13. M. Bohn. R. Lustig. J. Fischer. "Description of polyatomic real substances by two-center Lennard-Jones model fluids". *Fluid Phase Equilibria*. Vol. 25. 1986. pp. 251-262.
14. T. Tokumasu, K. Kamijo. "Molecular dynamics study for the thermal conductivity of diatomic liquid". *Superlattices and Microstructures*. Vo. 35. 2004. pp. 217-225.
15. I. Urukova, J. Vorholz, G. Maurer. "Solubility of CO2, CO, and H2 in the ionic liquid BMIMPF6 from monte carlo simulations". *J. Phys. Chem. B*. Vol. 109. 2005. pp. 12154-12159.
16. B. Berne, G. Harp. "On the Calculation of time correlation functions". *Advan. Chem. Phys*. Vol. 17. 1970. pp. 63-227.
17. M. Leeuwen. "Derivation of Stockmayer potential parameters for polar fluids". *Fluid Phase Equilibria*. Vol. 99. 1994. pp. 1-18.
18. J. Stoll, J. Vrabec, H. Hasse. "A set of molecular models for carbon monoxide and halogenated hydrocarbons". *J. Chem. Phys*. Vol. 119. 2003. pp. 11396-11407.
19. J. Bouanich, A. Predoi. "Theoretical calculations for line-broadening and pressure-shifting in the

fundamental and first two overtone bands of CO–H2". *J. Molec. Struct*. Vol. 742. 2005. pp. 183-190.

20. M. Bojan, W. Steele. "Interactions of diatomic molecules with graphite". *Langmuir*. Vol. 3. 1987. pp. 1123-1127.

21. J. Kottalam, D. Case. "Dynamics of ligand escape from the heme pocket of myoglobin". *J. Am. Chem. Soc.* Vol. 110. 1988. pp. 7690-7697.

22. R. Elber, M. Karplus. "Use of the time-dependent Hartree approximation for a simulation of carbon monoxide diffusion through myoglobin". *J. Am. Chem. Soc*. Vol. 112. 1990. pp. 9161-9175.

23. S. Pałucha, Z. Gburski, J. Biesiada. "A molecular dynamics study of fullerene–carbon monoxide mixture". *J. Molec. Struc*. Vol. 704. 2004. pp. 269-273.

24. K. Mirsky. "Carbon monoxide molecules in an argon matrix: empirical evaluation of the Ar·Ar, C·Ar and O·Ar potential parameters". *Chem. Phys*. Vol. 46. 1980. pp. 445-455.

25. M. Bojan, W. Steele "Virial coefficients for N2 and CO adsorbed on the graphite basal plane Elektronische". *Langmuir*. Vol. 3. 1987. pp. 116-120.

26. J. Straub, M. Karplus. "Molecular dynamics study of the photodissociation of carbon monoxide from myoglobin: Ligand dynamics in the first 10 ps". *Chem. Phys*. Vol. 158. 1991. pp. 221-248.

27. D. Nutt, M. Meuwly. "Theoretical Investigation of Infrared Spectra and Pocket Dynamics of Photodissociated Carbonmonoxy Myoglobin". *Biophys. J*. Vol. 85. 2003. pp. 3612-3623.

28. P. Fracassi, R. Valle. "Potential models and torsional stability in molecular crystals". *Chem. Phys. Lett*. Vol. 104. 1984. pp. 435-439.

29. P. Fracassi, R. Righini, R. Valle, M. Klein. "Lattice dynamics of solid α-carbon monoxide". *Chem. Phys*. Vol. 96. 1985. pp. 361-369.

30. M. Allen, D. Tildesley. *Computer simulation of liquids*. 1st ed. Ed. Oxford University Press. New York, USA. 1987. pp. 20-23.

31. D. Frenkel, B. Smit. *Understanding Molecular Simulation*. 1st ed. Ed. Academic Press. San Diego, USA. 2002. pp. 201-223.

32. P. Linstrom, W. Mallard. *NIST Standard Reference Database Number 69*. NIST Chemistry WebBook, National Institute of Standards and Technology. Available on: http://webbook.nist.gov. Accessed: November 18, 2009.